CRYSTAL GROWTH & DESIGN

pubs.acs.org/crystal

Article

High-Performance Piezoelectric Generator Based on a Monocrystalline $LiNbO_3$ Fiber

Raphael Victor Barros Campos, Francisco Enilton Alves Nogueira,* João Paulo Costa do Nascimento,* Felipe Felix do Carmo, Marcelo Antonio Santos da Silva, Sergio Paulo Marcondes, Antonio C. Hernandes, Svetlana V. Boriskina, Luis Marcelo Lozano Sánchez, and Antonio Sergio Bezerra Sombra

Cite This: *Cryst. Growth Des.* 2025, 25, 672−679

Read Online

ACCESS | Metrics & More | Article Recommendations

ABSTRACT: Energy harvesting from mechanical compression and stretching movements is an effective strategy for powering electronic devices. Piezoelectric materials are robust and can be activated by small movements or physical disturbances across various frequencies. With this in mind, the present study proposes the fabrication of monocrystalline lithium niobate ($LiNbO_3$) piezoelectric fibers, grown using the laser-heated pedestal growth (LHPG) technique and their application as high-efficiency energy converters. Electrical power generation was observed in response to mechanical deformations applied to the fabricated monocrystalline piezoelectric generator (PG). Under compression and stretching deformations of the $LiNbO_3$ piezoelectric monocrystalline fiber, one can find electric power generation in the range of 9.85 to 32.41 μW for stretching, and 19.55 μW at 34.13 μW for compression, with the application of 1 V. These results underscore the efficiency of monocrystalline lithium niobate ($LiNbO_3$) fibers in converting ambient mechanical energy into electrical energy, positioning them as a viable and environmentally friendly (lead-free materials) alternative to traditional piezoelectric materials in energy harvesting devices.

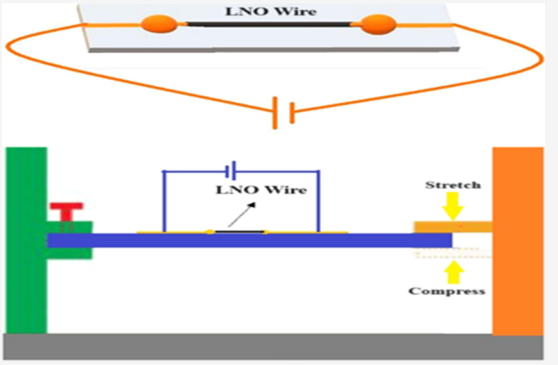

1. INTRODUCTION

Energy harvesting devices have long been pursued to power sensor networks and mobile devices without a battery. Piezoelectric crystals, which can generate electrical charges when mechanically deformed, are among the most promising materials for the development of energy harvesting devices. Based upon the energy conversion by the material's piezoelectricity, the piezoelectric generator (PG) is based on a piezoelectric monocrystal fiber (PCF) power generator that transforms ambient mechanical energy into a useful form of electrical energy.[1−4]

The search for energy harvesting devices has become a dynamic research field driven by the increasing demand for battery-independent powering of sensor networks and mobile devices. In this context, piezoelectric materials play a crucial role due to their ability to convert mechanical energy into electrical energy.[5−9] $LiNbO_3$ (LNO) is highly valued for its excellent piezoelectric response, especially in the d_{33} mode, which makes it ideal for the efficient conversion of ambient mechanical energy into usable electrical power.[10,11] The functionality of piezoelectric generators (PGs) based on single-crystalline piezoelectric fibers (PCFs) depends on their ability to transform mechanical energy into electrical energy. When deformed by external forces, PCFs generate a piezoelectric potential, causing electrons to flow and balance this potential.[12,13]

Recent studies on LNO have focused on energy harvesting, exploring innovative fabrication methods, such as electrospinning of monocrystalline fibers, and incorporating nanomaterials to improve performance.[14] One notable technique is the laser-heated pedestal growth (LHPG) method, which produces high-quality oxidized crystalline fibers.[15,16] This method allows rapid growth due to the high axial thermal gradient.[17−19] These technological advances have paved the way for devices that can efficiently capture and convert mechanical energy, contributing to sustainable and energy-sufficient technologies.[20]

In this article, we propose to investigate the performance of monocrystalline piezoelectric $LiNbO_3$ (LNO) fiber devices, which involves measuring electrical parameters, such as

Received: October 21, 2024
Revised: December 27, 2024
Accepted: December 30, 2024
Published: January 10, 2025

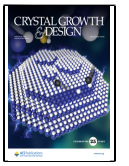

impedance (|Z|) and current (I), at different frequencies and mechanical conditions, including plane strain, tensile strain, and compressive strain. These results are essential to understand the energy conversion efficiency and the material response to various mechanical loads. This detailed characterization allows optimizing the device design to maximize power generation while ensuring stability and efficiency.

2. EXPERIMENTAL SECTION

The laser-heated pedestal growth (LHPG) technique was used to obtain the crystalline $LiNbO_3$ fibers used in this study. $LiNbO_3$ was prepared by mechanically mixing the reagents Li_2CO_3 (Vetec, 99% purity), Nb_2O_5 (Vetec, 99% purity), and poly(vinyl alcohol) (PVA).

A 125-Evolution-CO_2 laser at 10.6 μm was employed as a source of heat for the process of obtaining monocrystalline fibers $LiNbO_3$ in the LHPG system, whereas fibers were grown in an air atmosphere along the c-crystallographic axis.

Figure 1 shows the LHPG growth system, where it is possible to observe the experimental setup of axial temperature measurement along the pedestal/molten zone/fiber structure. Regarding the $LiNbO_3$ pedestal, it was synthesized using the solid-state technique and shaped into a cylindrical form through cold extrusion. Seed rods were also produced from the same pedestal and employed in the growth process.

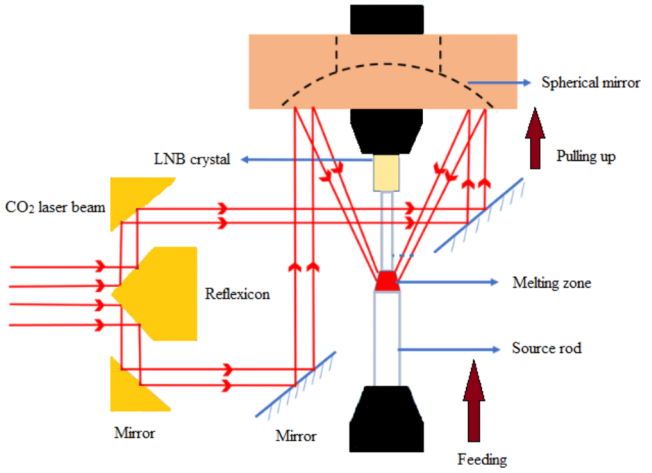

Figure 1. Schematic representation of the laser-heated pedestal growth (LHPG) technique.

The pedestal was pushed toward the molten zone, where the burnout of the binder (PVA), the decomposition of Li_2CO_3, the reaction of the starting materials, the sintering of $LiNbO_3$, and the growth of a stable monocrystalline fiber were carried out in a single operation.[21,22] Equation 1 correlates the pedestal radius and the fiber radius with the growth rate; and this expression was employed to estimate the required fiber radius:

$$R_F \approx R_P \sqrt{\frac{V_P}{V_F}} \quad (1)$$

R_F refers to the fiber radius, R_P refers to the pedestal radius, V_F and V_P refers to the growth speed and feed speed, respectively.

The structural analysis of the as-prepared materials was performed by XRD measurements using a diffractometer model (Rigaku D/max-B). The diffraction patterns were obtained in a range of 20−100° with an incident wavelength (Cu−Kα1) equal to 1.5443 Å, working at 40 kV and 40 mA, with a scan step of 0.013°.

The Raman spectra of the samples were recorded on a LabRAM HR HORIBA spectrometer using an argon ion laser with a wavelength of 488 nm operating at 2.54 eV as the excitation source. To focus the beam on the samples, an optical lens with a magnificence of 100×, and a numerical aperture of 0.90 was used as well as a grid with a density of 1800 lines/mm.

3. PIEZOELECTRIC THEORY

In the theory of piezoelectricity, the equations that describe the mechanical behavior of materials are connected to the equations that describe electric charges through piezoelectric constants. These constants are essential to characterizing how piezoelectric materials respond simultaneously to electrical and mechanical stimuli. The electromechanical coupling factor, such as k_{33}^2, is an important indicator of the efficiency with which these materials convert mechanical energy into electrical energy and vice versa. This coupling is essential for several technological applications, from sensors to power generation devices.[20]

Piezoelectric energy harvesting devices, such as piezoelectric generators, utilize the ability of piezoelectric materials to convert mechanical energy into electrical energy. These devices' efficiency depends on the material's piezoelectric response and its intrinsic "ability" to maximize mechanical deformation. In the case of $LiNbO_3$ crystal fiber, its monocrystalline structure allows an optimized anisotropic response to efficiently convert mechanical energy into electrical energy under different deformation conditions.[11−13] The deformation eq 2 for a material under tension is expressed as

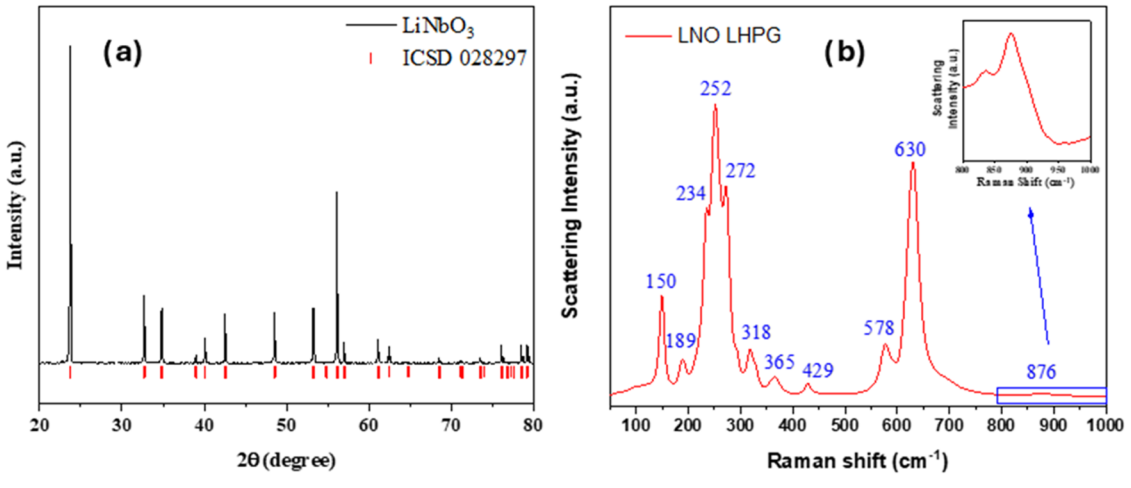

Figure 2. (a) XRD powder pattern of $LiNbO_3$ synthesized by the LHPG method and (b) Raman spectra of the LNO ($LiNbO_3$) LHPG fiber.

https://doi.org/10.1021/acs.cgd.4c01447
Cryst. Growth Des. 2025, 25, 672−679

$$\epsilon = 3\frac{a}{l}\left(\frac{D_{max}}{l}\right)\left(1 - \frac{z}{l}\right) \quad (2)$$

where a is half the substrate thickness, l is the length of the substrate from the fixed point to the free point of the polystyrene, D_{max} is the maximum strain at the free end, and z is the distance measured from the fixed point to the middle of the fiber. This equation indicates that the relationship between the strain ϵ and the maximum strain D_{max} is linear, allowing a uniform distribution of the strain along the fiber, essential for an accurate analysis of the piezoelectric response.[2]

4. RESULTS

The XRD and Raman spectra powder pattern results of $LiNbO_3$ synthesized by the LHPG method are shown in Figure 2a,b, respectively. The XRD pattern exhibits sharp diffraction peaks, where all of the peaks can be well indexed to the ferroelectric phase $LiNbO_3$ (ICSD No. 028297; space group: $R3c$). No additional peaks of other phases have been found, indicating the formation of a pure $LiNbO_3$ phase under such experimental conditions. Figure 3 shows the Raman spectra of the $LiNbO_3$

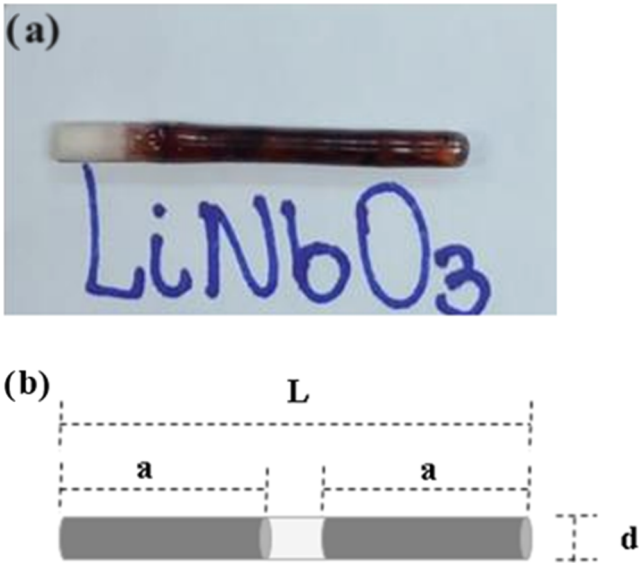

Figure 3. (a) $LiNbO_3$ fiber grown by the LHPG method. (b) Electrode and fiber geometry.

LHPG fiber at room temperature from 50 to 1000 cm^{-1}. The vibrational modes found at 150, 189, 234, and 252 cm^{-1} (E-TO modes) were assigned to the deformation of the NbO_6 framework. Raman peaks at 429 and 365 cm^{-1} (E-TO) were associated with the bending modes of the Nb−O−Nb bond. The Raman band centered at 630 cm^{-1} (A_1-TO) corresponded to the symmetric stretching of Nb−O−Nb bonds, while the Raman band above 876 cm^{-1} was assigned to the antisymmetric stretching of the Nb−O−Nb bonds in the NbO_6 octahedra in the rhombohedral $LiNbO_3$ and is attributed to the quasi longitudinal optical (E-LO) phonon mode. Bands centered at 303, 318, 326, and 578 cm^{-1} were also found.

For electrical measurements, the fabricated LNO fiber shown in Figure 3a shows that the fibers are free of cracks, demonstrating the efficiency of growing via the LHPG method. Figure 3b shows the fiber coated with silver paint electrodes for electrical measurements, where its dimensions are shown in Table 1.

Table 1. Monocrystalline $LiNbO_3$-Used Fiber

sample LNO	
L (mm)	6.87
d (mm)	0.89
a (mm)	3.0

Figure 4a,b shows the experimental setup used to apply mechanical stress in the fiber. Figure 4a shows the fiber under

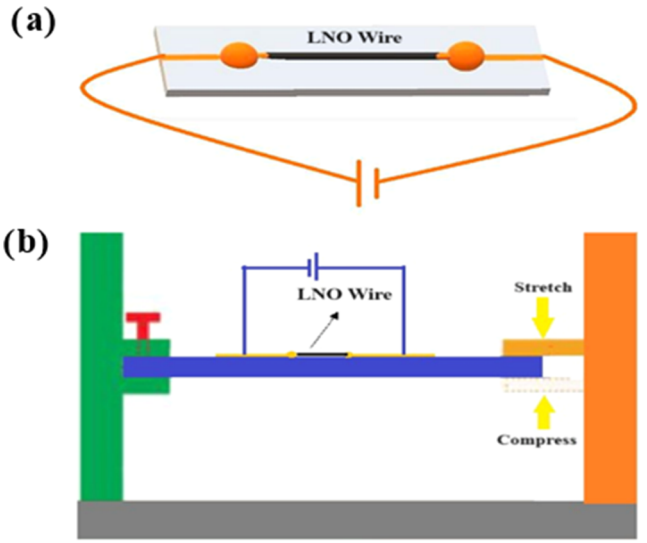

Figure 4. (a) LNO fiber on the polymer plate with electrical contacts. (b) Schematic diagram of the measurement system to characterize the properties of the piezoelectric generator (PG).

the polystyrene substrate and the electrode connections; the substrate is fixed at one end, while the other is fixed to a moving surface controlled with a stepper motor, as shown in Figure 4b. This arrangement allowed the application of periodic torsional and compression movements to the fiber. The motor control allowed us to produce precise and repeatable mechanical stresses, ensuring uniform mechanical stress during the vibration cycles.

The electrical properties of the fiber generator were evaluated using an HP4194A impedance/gain-phase analyzer, capable of measurements from 40 Hz to 110 MHz. The fibers were connected to the impedance analyzer, and electrical measurements were conducted in the frequency domain to evaluate parameters, such as impedance (|Z|). Initially, a study was carried out only with flat geometry (no applied deformation) with a voltage variation of 0.1 to 1 V in a frequency range of 40 Hz to 1 MHz, where it is possible to verify the influence of the voltage on the piezoelectric fiber.

In Figure 5, the variation of the current for the different voltages applied to the LNO fiber is observed for the entire analyzed spectrum, whereas a gradual increase in the current is observed with the increase of the applied voltage. It is observed that throughout the spectrum and at all applied voltages, the current continues to increase linearly as the frequency increases, except for frequencies close to 540 kHz which presents a slight distortion in the graph, a fact that is explained because it is at this frequency that the LNO fiber presents its piezoelectric resonance.

The relationship between the applied voltage and the resulting current at different frequencies is shown in Figure 6.

https://doi.org/10.1021/acs.cgd.4c01447
Cryst. Growth Des. 2025, 25, 672−679

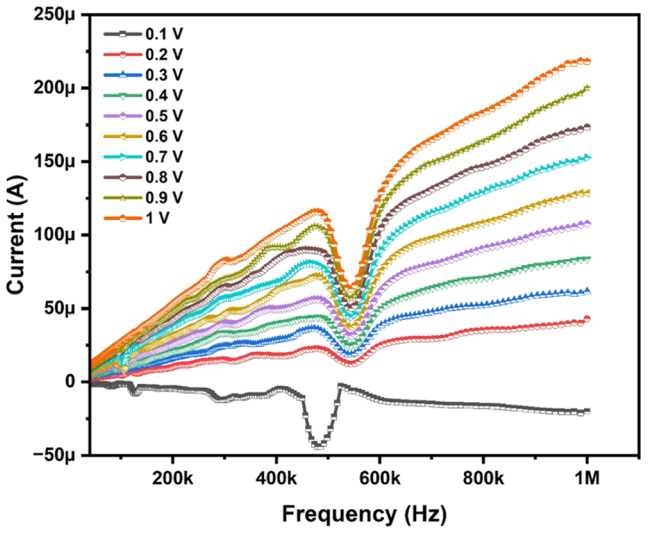

Figure 5. Current vs frequency in a range from 40 Hz to 1 M for different applied voltages.

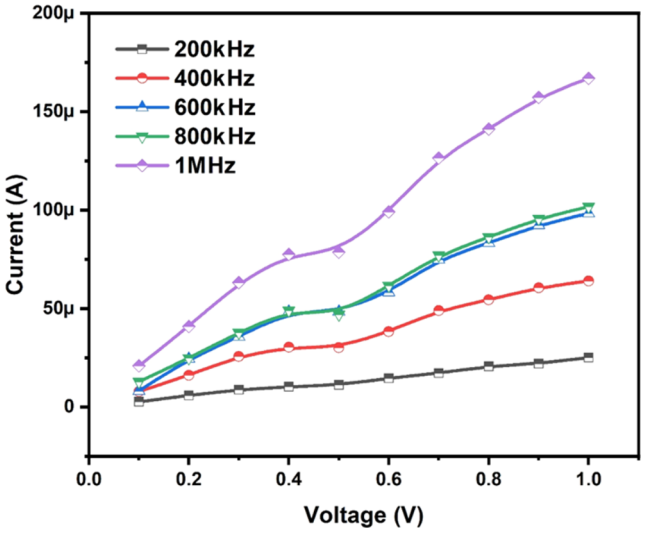

Figure 6. Current vs voltage at selected frequencies.

It is observed that for a low voltage range (0.1 to 0.4 V), the current increases linearly with the voltage, which indicates that the material follows Ohm's law and presents a mainly resistive behavior. This suggests that, at low voltages, the conduction mechanisms are dominated by direct ohmic conduction, without the presence of significant polarization or resonance effects.

As the voltage increases above 0.5 V, the increase in current is at a different growth rate, suggesting the presence of nonlinear conduction mechanisms. These effects may be related to charge carrier saturation or space charge limited conduction, where the charge density in the material begins to affect the current flow in a nonlinear manner. The existence of these effects at higher voltages indicates that the $LiNbO_3$ fiber has a slight nonlinear behavior in the electrical response.

For the study of mechanical deformations, including tensile deformation (stretching), compressive deformation, and mechanical vibration (twisting and compression), two different electrical voltages, 0.5 and 1 V, were used. For the starting configuration, the measurements were done without applying any external mechanical force. The changes in their corresponding electrical properties were recorded under tensile deformation conditions.

The impedance versus frequency plots at 0.5 V are shown in Figure 7a,b for compression and stretching, respectively. The results indicate that compression (C) decreases the impedance at frequencies around 540 kHz while stretching (S) increases the impedance, in relation to the flat configuration. The applied deformation makes it possible to calculate how much electric current is generated when there is a deformation in the piezoelectric fiber.

By analyzing the current results shown in Figure 8a,b, we observed that the current variations increase gradually with compression. The current tends to show specific peaks as compression increases, suggesting a sensitive response of the LNO monocrystal fiber to the applied force. Stretching also causes variations in the current but less intensely than compression. The amplitudes of the peaks are smaller, which may indicate that the response of the LNO to stretching is less pronounced at lower voltages.

The impedance response under 1 V application follows trends similar to those observed at 0.5 V but with larger amplitudes, as shown in Figure 9a,b. Compression further decreases the

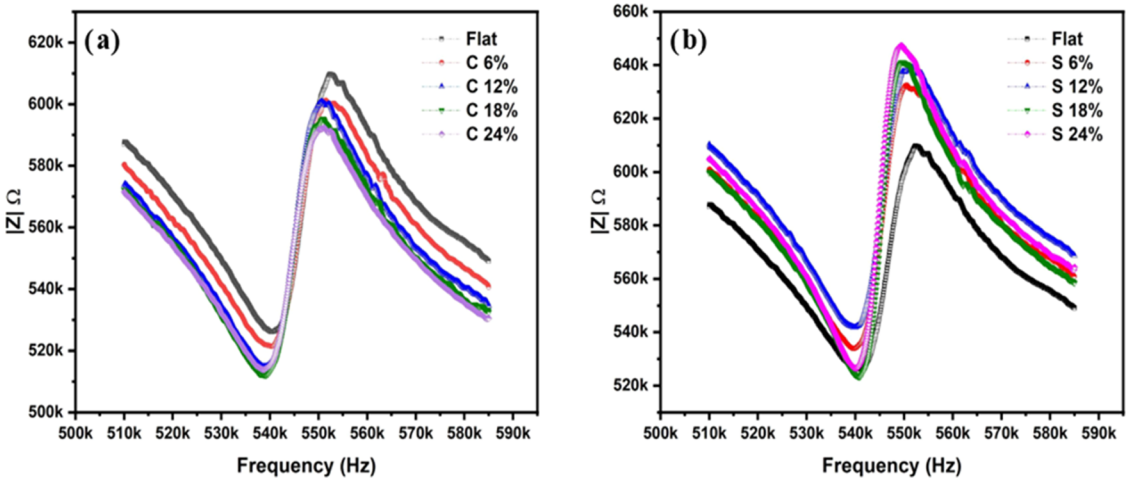

Figure 7. Impedance spectra at 0.5 V for (a) compression (C) and (b) stretching (S).

https://doi.org/10.1021/acs.cgd.4c01447
Cryst. Growth Des. 2025, 25, 672−679

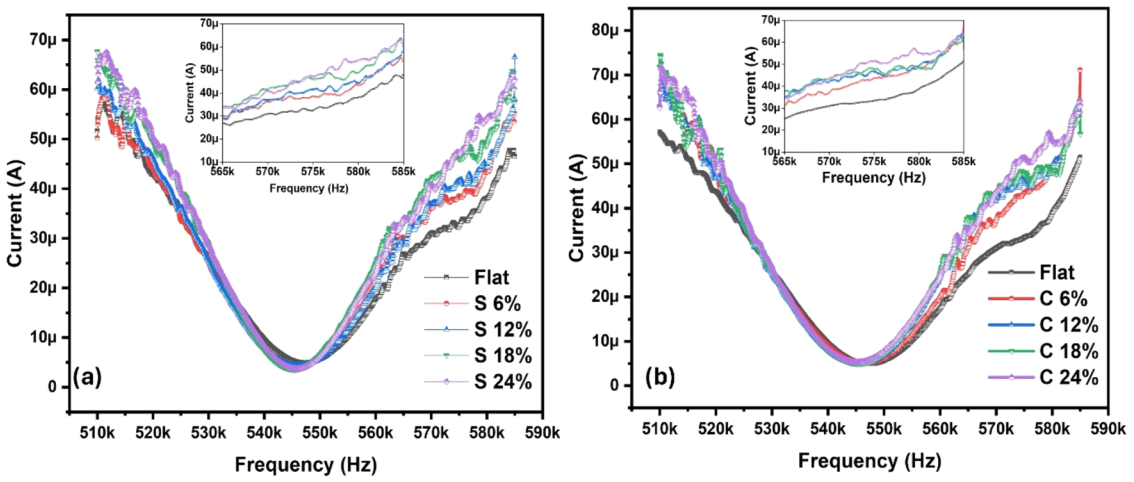

Figure 8. Current spectrum at 0.5 V for (a) compression (C) and (b) stretching (S).

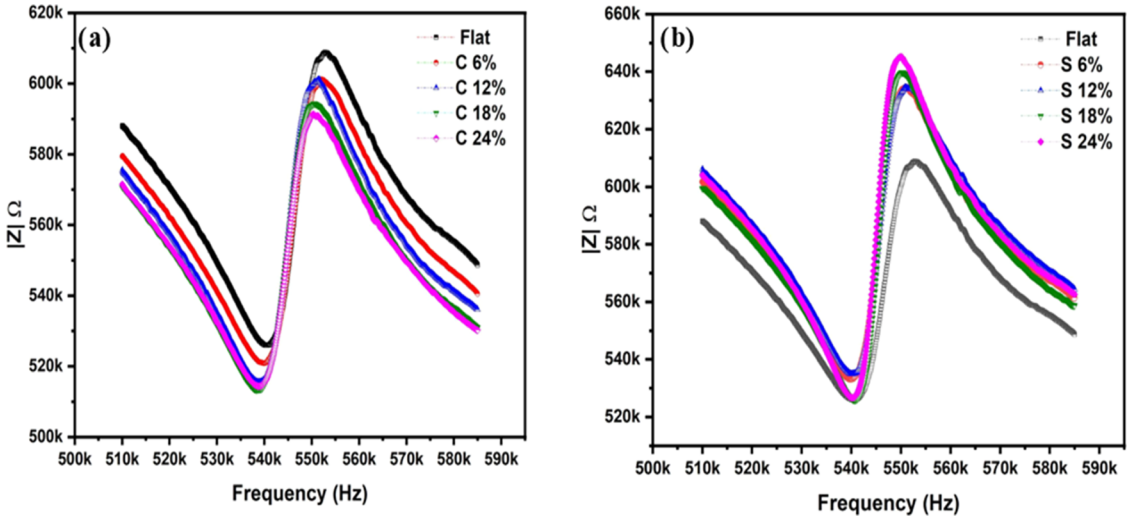

Figure 9. Impedance spectra at 1 V for (a) compression (C), and (b) stretching (S).

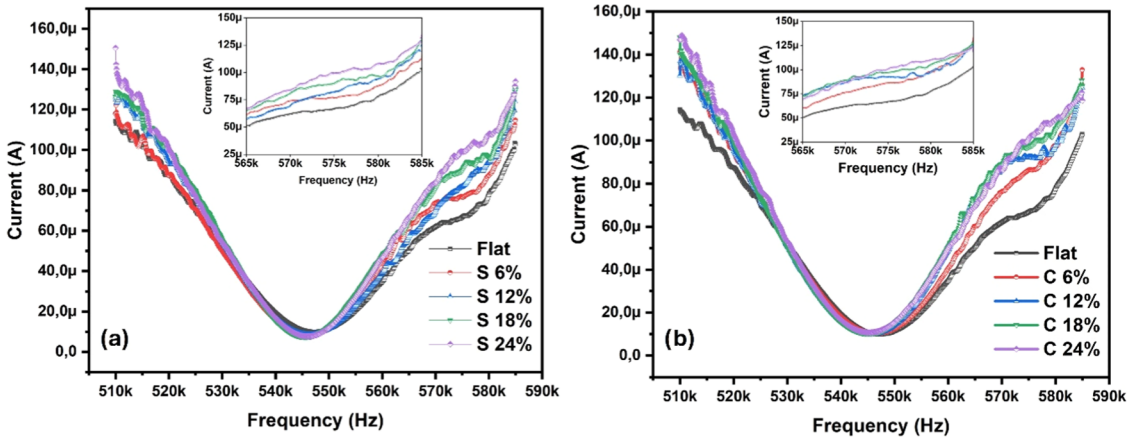

Figure 10. Current spectrum at 1 V for (a) compression (C) and (b) stretching (S).

impedance at frequencies close to 575 kHz, while stretching results in a significant increase in impedance, especially at higher frequencies.

The current response at 1 V is significantly more pronounced, with higher peaks compared with the measurements at 0.5 V, as shown in Figure 10a,b. This indicates that the LNO monocrystal exhibits a higher sensitivity to compression at higher strains, which can be attributed to the amplification of the piezoelectric effect with an increasing electric field. As with compression, stretching at 1 V generates higher peaks in the current. Higher stretching (18% and 24%) appears to induce significantly stronger responses at 1 V, suggesting that strain amplifies the

https://doi.org/10.1021/acs.cgd.4c01447
Cryst. Growth Des. 2025, 25, 672−679

mechanoelectrical response for both compression and stretching, as can be more clearly observed in Table 2.

Table 2. Variation of Currents for an Electric Field of 0.5 and 1 V for Stretching (S) and Compression (C)

condition	current (μA) at 0.5 V	current (μA) at 1 V	frequency (kHz) at (0.5 V)/(1 V)
S 6%	38.50	76.60	575
S 12%	41.62	82.05	575
S 18%	45.96	90.07	575
S 24%	47.17	99.16	575
C 6%	43.58	86.30	575
C 12%	46.39	92.46	575
C 18%	47.60	97.18	575
C 24%	51.28	100.88	575

Table 2 shows the current and corresponding frequencies for excitation voltages of 0.5 and 1 V, applied under various mechanical deformations in the LNO crystal fiber. A frequency of 575 kHz was chosen for the study. It is observed that, under stretching and compression conditions, the current values increase consistently with increasing deformation, both for voltages of 0.5 and 1 V. This behavior indicates that the LNO monocrystal fiber responds directly to the increase in mechanical elongation with a higher current generation.

The increase in current is most pronounced at 1 V, which is expected since a higher excitation voltage generates a stronger electric field, amplifying the material's piezoelectric response. For a stretching of 6%, the peak current is 38.50 μA at 0.5 V and 76.60 μA at 1 V, while for a stretching of 24%, these values rise to 47.17 and 99.16 μA, respectively. This trend amplifies the electrical response as the stress and strain increase.

Table 3 shows the generated power under different deformations for voltages of 0.5 and 1 V. The power variation

Table 3. Power Generation under Compression and Stretching Conditions at 0.5 and 1 V for Stretching (S) and Compression (C)

condition	power generation (μW) at 0.5 V	power generation (μW) at 1 V
S 6%	3.02	9.85
S 12%	4.58	15.30
S 18%	6.75	23.32
S 24%	7.35	32.41
C 6%	5.56	19.55
C 12%	6.96	25.71
C 18%	7.57	30.43
C 24%	9.41	34.13

measures the generated energy by the piezoelectric monocrystal fiber under mechanical deformation. To calculate the generated power, the difference between the flat power and the power generated by the applied deformations was calculated. The power variation for both stretching and compression tends to increase with increasing deformation, being more expressive at 1 V. For example, during a 6% elongation, the power variation is 3.02 μW at 0.5 V and 9.85 μW at 1 V. This trend is repeated for all deformation percentages, highlighting how the electromechanical energy generated by the material is amplified by the higher excitation voltage.

With the study carried out, it can be observed that the LNO monocrystal fiber can function as a high-performance and efficient generator. Table 4 shows a comparison of the power generated by other materials used as power generators. For

Table 4. Comparison of Generated Power

material	reference	power generation (μW)
PZT	10	0.03
$BaTiO_3$	25	0.18
ZnO	26	20
PVDF	27	2.28
$ZnSnO_3$	28	10.80
LNO	present work	34.13

comparison, the power generated with the application of a 24% compression deformation was selected. It is possible to observe that the power values generated by the LNO fiber presented here are close to or higher than those presented by many materials published in the literature, demonstrating that this material would be a candidate with a high potential as a piezoelectric power generator. The results of this study demonstrate that single-crystalline $LiNbO_3$ fibers exhibit superior performance compared with polycrystalline materials. This is because the absence of grain boundaries in single-crystalline fibers eliminates energy losses associated with domain misalignment and interactions at these boundaries, problems frequently observed in polycrystals. As pointed out by previous research, polycrystalline materials tend to present intrinsic structural defects, such as lithium (Li) vacancies, which negatively affect properties, such as electrical polarization and piezoelectric efficiency.[23,24]

5. CONCLUSIONS

In this study, monocrystalline $LiNbO_3$ (LNO) fibers were successfully grown using the laser-heated pedestal growth (LHPG) technique, which proved to be highly efficient in producing crack-free fibers. Structural characterization by Raman spectroscopy and X-ray diffraction confirmed the crystalline structure of the fibers and formation of the pure LNO phase. Experimental results revealed resonance frequencies at around 540 kHz. The fabricated fibers were tested as piezoelectric generators (PG), where mechanical deformations generated electrical energy. Compression and stretching deformations, combined with the application of an electric tension of 0.5 and 1 V, demonstrated an increase in electrical power with greater applied deformation. Electric power generation ranged from 9.85 to 34.13 μW under compression and stretching deformations with the application of 1 V. These findings highlight the potential of LNO monocrystalline fibers as piezoelectric generators for powering electronic devices.

AUTHOR INFORMATION

Corresponding Authors

Francisco Enilton Alves Nogueira − *Telecommunication Engineering Department, Federal University of Ceará (UFC), 60.755-640 Fortaleza, Ceará,, Brazil; Telecommunication and Materials Science and Engineering of Laboratory (LOCEM), http://www.locem.ufc.br, Physics Department, Federal University of Ceará (UFC), 60.440-554 Fortaleza, Ceará,, Brazil*; Email: fenilton@gmail.com

João Paulo Costa do Nascimento − *Federal Institute of Education, Science and Technology of Ceara, PPGET, 60.040-531 Fortaleza, Ceará, Brazil; Telecommunication and Materials Science and Engineering of Laboratory (LOCEM), http://www.locem.ufc.br, Physics Department, Federal*

https://doi.org/10.1021/acs.cgd.4c01447
Cryst. Growth Des. 2025, 25, 672−679

University of Ceará (UFC), 60.440-554 Fortaleza, Ceará,, Brazil; orcid.org/0000-0002-6236-7284;
Email: jpquimico3@gmail.com

Authors

Raphael Victor Barros Campos − *Telecommunication Engineering Department, Federal University of Ceará (UFC), 60.755-640 Fortaleza, Ceará,, Brazil; Telecommunication and Materials Science and Engineering of Laboratory (LOCEM), http://www.locem.ufc.br, Physics Department, Federal University of Ceará (UFC), 60.440-554 Fortaleza, Ceará,, Brazil*

Felipe Felix do Carmo − *Department of Organic and Inorganic Chemistry, Federal University of Ceará (UFC), 60.440-900 Fortaleza, Ceará, Brazil; Telecommunication and Materials Science and Engineering of Laboratory (LOCEM), http://www.locem.ufc.br, Physics Department, Federal University of Ceará (UFC), 60.440-554 Fortaleza, Ceará,, Brazil*

Marcelo Antonio Santos da Silva − *Telecommunication and Materials Science and Engineering of Laboratory (LOCEM), http://www.locem.ufc.br, Physics Department, Federal University of Ceará (UFC), 60.440-554 Fortaleza, Ceará,, Brazil*

Sergio Paulo Marcondes − *São Carlos Institute of Physics, University of São Paulo, 13560-970 São Carlos, SP, Brazil;* orcid.org/0009-0006-8274-7272

Antonio C. Hernandes − *São Carlos Institute of Physics, University of São Paulo, 13560-970 São Carlos, SP, Brazil*

Svetlana V. Boriskina − *Department of Mechanical Engineering, Massachusetts Institute of Technology (MIT), Cambridge, Massachusetts 02139, United States*

Luis Marcelo Lozano Sánchez − *Department of Mechanical Engineering, Tecnológico de Monterrey, 64849 Monterrey, N.L.,, México;* orcid.org/0000-0003-1902-5550

Antonio Sergio Bezerra Sombra − *Telecommunication and Materials Science and Engineering of Laboratory (LOCEM), http://www.locem.ufc.br, Physics Department, Federal University of Ceará (UFC), 60.440-554 Fortaleza, Ceará,, Brazil*

Complete contact information is available at:
https://pubs.acs.org/10.1021/acs.cgd.4c01447

Funding

This work was partly sponsored by the Brazilian Research Agencies CNPq-Conselho Nacional de Desenvolvimento Científico e Tecnológico (Grant INCT NANO(BIO)SIMES), CAPES- Coordenação de Aperfeiçoamento de Pessoal de Ensino Superior (Grant Project PNPD), FINEP-Financiadora de Estudos e Projetos (Grant INFRAPESQ-11 and INFRAPESQ-12), and the Office of Naval Research Global (N62909-23-1-2109).

Notes

The authors declare no competing financial interest.

REFERENCES

(1) Jung, J. H.; Lee, M.; Hong, J.-I.; Ding, Y.; Chen, C.-Y.; Chou, L.-J.; Wang, Z. L. Lead-Free NaNbO 3 Nanowires for a High Output Piezoelectric Nanogenerator. *ACS Nano* **2011**, *5* (12), 10041−10046.

(2) Wang, Z.; Qi, J.; Yan, X.; Zhang, Q.; Wang, Q.; Lu, S.; Lin, P.; Liao, Q.; Zhang, Z.; Zhang, Y. A Self-Powered Strain Senor Based on a ZnO/PEDOT:PSS Hybrid Structure. *RSC Adv.* **2013**, *3* (38), 17011.

(3) Lee, T. Il.; Lee, S.; Lee, E.; Sohn, S.; Lee, Y.; Lee, S.; Moon, G.; Kim, D.; Kim, Y. S.; Myoung, J. M.; Wang, Z. L. High-Power Density Piezoelectric Energy Harvesting Using Radially Strained Ultrathin Trigonal Tellurium Nanowire Assembly. *Adv. Mater.* **2013**, *25* (21), 2920−2925.

(4) Wu, W.; Bai, S.; Yuan, M.; Qin, Y.; Wang, Z. L.; Jing, T. Lead Zirconate Titanate Nanowire Textile Nanogenerator for Wearable Energy-Harvesting and Self-Powered Devices. *ACS Nano* **2012**, *6* (7), 6231−6235.

(5) Zhou, J.; Gu, Y.; Fei, P.; Mai, W.; Gao, Y.; Yang, R.; Bao, G.; Wang, Z. L. Flexible Piezotronic Strain Sensor. *Nano Lett.* **2008**, *8* (9), 3035−3040.

(6) Shur, V. Y. Lithium Niobate and Lithium Tantalate-Based Piezoelectric Materials. In *Advanced Piezoelectric Materials*; Elsevier, 2010; pp 204−238 DOI: 10.1533/9781845699758.1.204.

(7) Fischer, A. C.; Forsberg, F.; Lapisa, M.; Bleiker, S. J.; Stemme, G.; Roxhed, N.; Niklaus, F. Integrating MEMS and ICs. *Microsyst. Nanoeng.* **2015**, *1*, No. 15005, DOI: 10.1038/micronano.2015.5.

(8) Zhu, Q.; Song, X.; Chen, X.; Li, D.; Tang, X.; Chen, J.; Yuan, Q. A High Performance Nanocellulose-PVDF Based Piezoelectric Nanogenerator Based on the Highly Active CNF@ZnO via Electrospinning Technology. *Nano Energy* **2024**, *127* (January), No. 109741.

(9) Toprak, A.; Tigli, O. MEMS Scale PVDF-TrFE-Based Piezoelectric Energy Harvesters. *J. Microelectromech. Syst.* **2015**, *24* (6), 1989−1997.

(10) Xu, S.; Hansen, B. J.; Wang, Z. L. Piezoelectric-Nanowire-Enabled Power Source for Driving Wireless Microelectronics. *Nat. Commun.* **2010**, *1* (1), No. 93.

(11) Habib, M.; Lantgios, I.; Hornbostel, K. A Review of Ceramic, Polymer and Composite Piezoelectric Materials. *J. Phys. D. Appl. Phys.* **2022**, *55* (42), No. 423002.

(12) Park, K.; Son, J. H.; Hwang, G.; Jeong, C. K.; Ryu, J.; Koo, M.; Choi, I.; Lee, S. H.; Byun, M.; Wang, Z. L.; Lee, K. J. Highly-Efficient, Flexible Piezoelectric PZT Thin Film Nanogenerator on Plastic Substrates. *Adv. Mater.* **2014**, *26* (16), 2514−2520.

(13) Wu, N.; Fu, J.; Xiong, C. A Bio-Inspired Bistable Piezoelectric Structure for Low-Frequency Energy Harvesting Applied to Reduce Stress Concentration. *Micromachines* **2023**, *14*, 909.

(14) Zhang, J.; Wang, X.; Zhang, Y. $LiNbO_3$ Crystal Intense Electric Field Sensor Coupled With Twisted Polarization Maintaining Fiber. *IEEE Trans. Instrum. Meas.* **2023**, *72*, No. 3293550.

(15) Fernández-Carrión, A. J.; Bourret, J.; Sharp, J.; Xing, M.; Duclère, J.-R.; Colas, M.; Cornette, J.; Carles, P.; Genevois, C.; Brisset, F.; Chenu, S.; Allix, M.; Delaizir, G. Elaboration and Luminescence Properties of Laser-Heated Pedestal Growth Sr 3 Al 2 O 6 -Based Fibers. *Cryst. Growth Des.* **2022**, *22* (11), 6828−6836.

(16) Wang, X.; Li, X.; Deng, M.; Zhang, Z.; Yang, F.; Kou, H.; Su, L.; Wu, A.; Chen, J. A Couple-Free Structured LuAG:Ce-LuAG Scintillating Single Crystal Fiber Grown by a Laser-Heated Pedestal Growth Method. *Cryst. Growth Des.* **2024**, *24* (8), 3333−3341.

(17) Maxwell, G.; Ponting, B.; Gebremichael, E.; Magana, R. Advances in Single-Crystal Fibers and Thin Rods Grown by Laser Heated Pedestal Growth. *Crystals* **2017**, *7*, No. 12.

(18) Wang, X.; Zhang, Z.; Li, X.; Kou, H.; Zhang, Z.; Dai, Y.; Zhou, S.; Wu, X.; Wu, Q.; Chen, J.; Su, L.; Wu, A. Light Response Uniformity of LuAG:Ce Scintillating Single Crystal Fiber Grown by Laser Heated Pedestal Growth Method. *Radiat. Meas.* **2023**, *169*, No. 107017.

(19) Enilton Alves Nogueira, F.; Victor Barros Campos, R.; Paulo Costa do Nascimento, J.; Felix do Carmo, F.; Antonio Santos da Silva, M.; Paulo Marcondes, S.; Carlos Hernandes, A.; Sergio Bezerra Sombra, A. Piezoelectric Temperature Acoustic Sensor of LiNbO3 Crystal Fibers Operating at Radio Frequencies. *J. Cryst. Growth* **2024**, *643* (April), No. 127799.

(20) Kim, H. S.; Kim, J. H.; Kim, J. A Review of Piezoelectric Energy Harvesting Based on Vibration. *Int. J. Precis. Eng. Manuf.* **2011**, *12*, 1129.

(21) Rueda-P, J. E.; Rodrigues, J. E. F. S.; Hernandes, A. C. Monocrystalline Fiber Growth Technique: New Critical Radius Considerations. *J. Cryst. Growth* **2021**, *570* (May), No. 126199.

(22) Andreeta, M. R. B.; Hernandes, A. C.Laser-Heated Pedestal Growth of Oxide Fibers. In *Springer Handbook of Crystal Growth* 2010; p 393 .
(23) Sánchez-Dena, O.; Fierro-Ruiz, C. D.; Villalobos-Mendoza, S. D.; Carrillo Flores, D. M.; Elizalde-Galindo, J. T.; Farías, R. Lithium Niobate Single Crystals and Powders Reviewed—Part I. *Crystals* **2020**, *10* (11), 973.
(24) Sánchez-Dena, O.; Villalobos-Mendoza, S. D.; Farías, R.; Fierro-Ruiz, C. D. Lithium Niobate Single Crystals and Powders Reviewed—Part II. *Crystals* **2020**, *10* (11), 990.
(25) Yan, J.; Jeong, Y. G. High Performance Flexible Piezoelectric Nanogenerators Based on BaTiO3 Nanofibers in Different Alignment Modes. *ACS Appl. Mater. Interfaces* **2016**, *8*, 15700.
(26) Wang, Z.; Liu, S.; Yang, Z.; Dong, S. Perspective on Development of Piezoelectric Micro-Power Generators. *Nanoenergy Adv.* **2023**, *3* (2), 73−100.
(27) Siddiqui, S.; Kim, D.-I.; Roh, E.; Duy, L. T.; Trung, T. Q.; Nguyen, M. T.; Lee, N.-E. A Durable and Stable Piezoelectric Nanogenerator with Nanocomposite Nanofibers Embedded in an Elastomer under High Loading for a Self-Powered Sensor System. *Nano Energy* **2016**, *30*, 434−442.
(28) Alam, M. M.; Ghosh, S. K.; Sultana, A.; Mandal, D. Lead-Free ZnSnO3/MWCNTs-Based Self-Poled Flexible Hybrid Nanogenerator for Piezoelectric Power Generation. *Nanotechnology* **2015**, *26*, No. 165403.

https://doi.org/10.1021/acs.cgd.4c01447
Cryst. Growth Des. 2025, 25, 672−679